ELSEVIER

Journal of Fluids and Structures 22 (2006) 885–895

JOURNAL OF FLUIDS AND STRUCTURES

www.elsevier.com/locate/jfs

Three distinct response regimes for the transverse Vortex-Induced Vibrations of circular cylinders at low Reynolds numbers

R.H.J. Willden*, J.M.R. Graham

Department of Aeronautics, Imperial College London, SW7 2AZ, UK

Received 21 November 2005; accepted 17 April 2006
Available online 24 July 2006

Abstract

The paper reports and discusses the results of a numerical investigation of the low-Reynolds-number transverse Vortex-Induced Vibrations (VIV) of low-mass-ratio elastically supported circular cylinders. Simulations were conducted over a large range of reduced velocities, from 2.5 to 20.0, at Reynolds numbers from 50 to 400. The objective of the study was to ascertain the dependency of the transverse vibrational behaviour of low-mass-ratio circular cylinders on their mass ratio. Simulations were conducted at mass ratios representative of a cylinder in water: 1, 2, 5 and 10, and for reference to higher mass ratio VIV at a mass ratio of 50. It was found that, at low Reynolds numbers, $Re \leqslant 400$, transversely vibrating circular cylinders exhibit three distinct regions of response: a primary response which occurs at and around resonance and is that normally associated with VIV, secondary or super-harmonically excited responses, and a tertiary, or infinite lock-in, response. The paper reports and discusses the response and vortex shedding characteristics of these three response regimes.

Keywords: Vortex-Induced Vibration; Circular cylinder; Computational fluid dynamics

1. Introduction

For all but the lowest Reynolds numbers the flow past a bluff body results in the asymmetric shedding of vortices into the body's wake. These vortices induce periodic forces on the body and can, if the body is elastically supported, cause it to vibrate. Such a vibration is termed a Vortex-Induced Vibration (VIV). VIV can provide a major source of fatigue damage to engineering structures and it is therefore imperative to predict the occurrence, and the likely amplitude and frequency, of VIV when designing structures that are exposed to current flows.

The flow-induced vibrations of many bluff bodies have been investigated, but by far the most research attention has been given to investigating the VIV of circular cylinders. This is in part due to the engineering importance of circular cross-section bodies. The fluid forces acting on a circular cylinder in both the cross-flow (transverse) direction, the lift, and the streamwise (in-line) direction, the drag, can cause VIV in their respective directions. The amplitude of transverse VIV, which can exceed a diameter, is normally greater than that of in-line VIV. Vortex excited bodies can

*Corresponding author. Tel.: +44 20 7594 5117; fax: +44 20 7584 8120.
E-mail address: r.willden@imperial.ac.uk (R.H.J. Willden).

0889-9746/$ - see front matter
doi:10.1016/j.jfluidstructs.2006.04.005

experience a nonlinear phenomenon known as lock-in, whereby the vortex shedding and oscillation frequencies become synchronized. This synchronization can lead to an increase in the spanwise correlation of the vortex shedding and a substantial amplification of the cylinder's vibrational response. Much of the recent research is discussed in the reviews by Sarpkaya (2004) and Williamson and Govardhan (2004).

The paper reports on a numerical investigation of the low-Reynolds-number transverse VIV of circular cylinders. The Reynolds number, $\mathrm{Re} = UD/\nu$ (where U, D and ν are the upstream flow speed, the cylinder diameter and the kinematic viscosity of the fluid, respectively), was varied between 50 and 400. Simulations were conducted at several mass ratios (the ratio of the cylinder's mass to the mass of fluid displaced by it): 1, 2, 5, 10 and 50, in order to ascertain the dependency of the cylinder's transverse vibrational behaviour on its mass ratio.

2. Numerical method

The evolution of the fluid flow is computed by solving the velocity–vorticity formulation of the two-dimensional incompressible Navier–Stokes equations. The nondimensional equation of motion is given by

$$\frac{\partial \omega}{\partial t} + (\mathbf{u} \cdot \nabla)\omega = \frac{1}{\mathrm{Re}} \nabla^2 \omega, \tag{1}$$

where $\mathbf{u}$, ω and t are the nondimensional velocity vector, spanwise component of vorticity and time. The characteristic length and speed used for nondimensionalization are the cylinder diameter, D, and the upstream flow speed, U. Eq. (1) is solved using a first-order time split approach, whereby the diffusion of vorticity is treated in an Eulerian fashion by modelling the flow variables using linear finite elements on an unstructured triangular element mesh, and the convection is handled using a Lagrangian approach that employs discrete point vortices.

The transverse response of the cylinder, $Y(t)$, to cross-flow fluid loading per unit span, $F_y(t)$, is modelled using a mass, spring and damper model. The cylinder's nondimensional equation of transverse motion is given by

$$\ddot{Y} + 2\beta \left(\frac{V_r}{2\pi}\right)^{-1} \dot{Y} + \left(\frac{V_r}{2\pi}\right)^{-2} Y = \frac{2}{\pi m^*} C_L, \tag{2}$$

where Y, $\dot{Y} = \mathrm{d}Y/\mathrm{d}t$ and $\ddot{Y} = \mathrm{d}^2 Y/\mathrm{d}t^2$ are the cylinder's nondimensional displacement, velocity and acceleration. $C_L = F_y/\frac{1}{2}\rho U^2 D$ is the cylinder's sectional lift coefficient and ρ is the fluid density (the sectional drag coefficient, C_D, is defined in an analogous manner). $V_r = U/f_n D$ is the reduced velocity, $\beta = c/2\sqrt{km}$ is the structural damping ratio, and $m^* = 4m/\pi\rho D^2$ is the mass ratio. m, c and k are the cylinder's mass, viscous damping and elastic stiffness per unit span, and $f_n = (1/2\pi)\sqrt{k/m}$ is the cylinder's natural frequency of vibration in vacuo.

The computation proceeds in a loosely coupled staggered fashion that alternately computes the evolution of the flow and the subsequent response of the cylinder to the computed fluid loading. The flow is computed in the body-fixed frame of reference by subjecting the cylinder to an onset flow that is the relative velocity of the flow to the cylinder in the inertial frame. For further details on the numerical method see Willden (2003).

All of the simulations presented in this paper were computed on an unstructured triangular element mesh comprising 26 943 elements and 13 679 nodes. The domain inflow and outflow boundaries were, respectively, located 25 diameters upstream and 50 diameters downstream of the cylinder's centre. The upper and lower surfaces of the mesh were positioned 25 diameters to either side of the cylinder's centre, yielding an effective blockage of 2%. The mesh resolution was varied in accordance with the expected variation in the spatial gradients of the flow variables, with the finest elements occurring adjacent to the cylinder and being of approximate dimension $0.01D$.

3. Transverse vibrations of low-mass-ratio elastically supported cylinders

Presented below is a low-Reynolds-number numerical investigation of the transverse vibrational behaviour of low-mass-ratio elastically supported circular cylinders. In all of the simulations presented the cylinder was constrained from moving in the in-line direction but was free to vibrate in the transverse direction. The objective of this study was to ascertain the dependency of the transverse vibrational behaviour of low-mass-ratio circular cylinders on their mass ratio. Simulations were conducted at mass ratios representative of a cylinder in water: 1, 2, 5 and 10, and for reference to higher mass ratio VIV at $m^* = 50$. In all of the simulations presented the structural damping ratio, β, was set to zero, in order that the maximum possible response be excited.

For each of the mass ratios considered the reduced velocity was varied from 2.5 to 20.0 in increments of 0.25. High-mass-ratio cylinders, $m^* = \mathcal{O}(10^2)$ say, exhibit VIV over a fairly narrow reduced velocity range; $4 \lesssim V_r \lesssim 8$ [e.g. see Feng (1968) or Anagnostopoulos and Bearman (1992)]. However, the upper reduced velocity at which low-mass-ratio cylinders, $m^* = \mathcal{O}(1)$ say, exhibit VIV is far greater [e.g. see Shiels et al. (2001), Willden and Graham (2001) or Govardhan and Williamson (2002)]. The present simulations were conducted up to $V_r = 20.0$ in order to capture any high reduced velocity responses experienced by the low-mass-ratio cylinders being considered.

Changes to the reduced velocity were achieved by altering the flow speed and with it therefore the Reynolds number. Throughout the present investigation $\mathrm{Re} = 20V_r$, such that the Reynolds number varied from 50 to 400. Above a Reynolds number of approximately 180, three-dimensional vortical structures are observed in the wake of a stationary circular cylinder (Williamson, 1996). However, it is known that an effect of lock-in is to substantially correlate the vortex shedding along the span of a vibrating cylinder (Toebes, 1969), rendering the fluid flow predominantly two-dimensional. The correlating effect of lock-in is used in the present study to justify the use of two-dimensional simulations to compute flows past vibrating cylinders at Reynolds numbers above 180.

At the start of each simulation, the cylinder, which was initially held at rest in its equilibrium position, i.e. $Y(0) = 0$ and $\dot{Y}(0) = 0$, was released and the flow started impulsively from rest. Each simulation was run for at least 1000, and up to 3000, convective time units, where D/U is the convective time unit. (Assuming a Strouhal number, $\mathrm{St} = f_s D/U$ where f_s is the Strouhal frequency, of 0.2 a stationary cylinder's shedding period is 5 convective time units in length). Each simulation was run for as long as was necessary to obtain an interval of adequate length (at least 500 convective time units) over which the solution was statistically invariant. This interval, which was taken from the final portion of each simulation, was used for analysing the simulation results.

3.1. Amplitude of response

The computed r.m.s. response amplitudes, $Y_{\mathrm{r.m.s}}$, of all five mass ratio cylinders considered are presented together in Fig. 1 as a function of the reduced velocity, V_r, and the Reynolds number, $\mathrm{Re} = 20V_r$. The highest mass ratio cylinder considered, $m^* = 50$, exhibits little or no response for $V_r \leqslant 5.0$. On increasing V_r past 5.0, the response amplitude rises sharply until a maximum r.m.s. response of $0.31D$ is obtained at $V_r = 5.75$. Following its maximum the response amplitude falls off rapidly with increasing V_r, and by $V_r = 6.5$ the response is again very low, $Y_{\mathrm{r.m.s}} \approx 0.01$. The response is confined to quite a narrow reduced velocity range, $5.0 < V_r < 6.5$, which is typical of moderate to high-mass-ratio VIV. The response is centred upon $V_r = 5.75 \approx 1/\mathrm{St}$. In the present text a response, such as that described above, that encompasses $V_r \approx 1/\mathrm{St}$ is referred to as the cylinder's *primary response*.

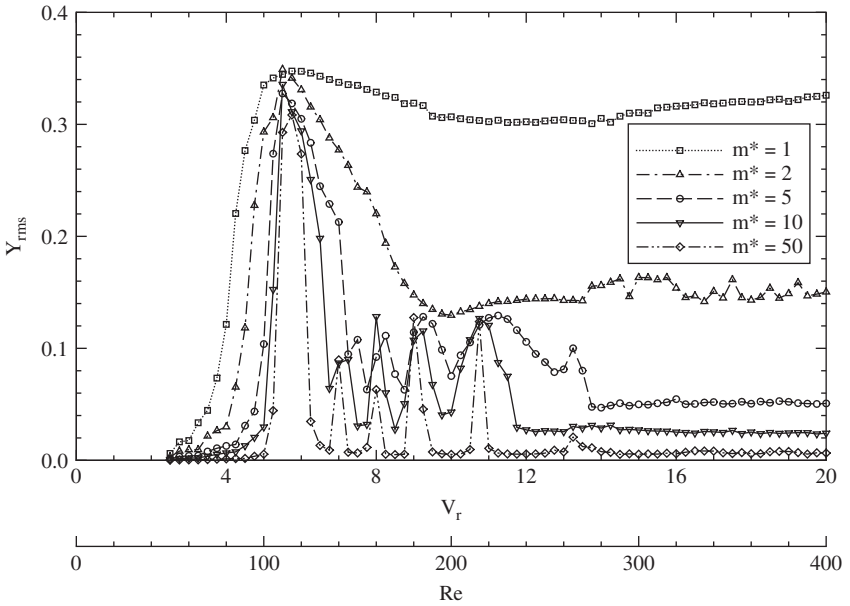

Fig. 1. Root-mean-square response amplitudes, $Y_{\mathrm{r.m.s}}$, as a function of the reduced velocity, V_r, and the Reynolds number, $\mathrm{Re} = 20V_r$, of transversely vibrating circular cylinders; $m^* = 1$, 2, 5, 10 and 50, and $\beta = 0$.

On increasing V_r beyond the upper extremity of the primary response region several narrow, in terms of V_r, *secondary responses* are encountered. These secondary responses are centred on $V_r = 7.0$, 8.0, 9.0 and 10.75, and each exhibits a lower maximum r.m.s. response amplitude, $Y_{\text{r.m.s}} \approx 0.1$, than is exhibited in the primary response region. At all higher reduced velocities, $V_r \geqslant 11.0$, the cylinder exhibits little or no response.

The most notable difference between the response of the $m^* = 10$ cylinder and the response of the $m^* = 50$ cylinder is that for the lower mass ratio cylinder the primary and secondary responses cover a wider range of reduced velocities. Below a reduced velocity of 4.5 the $m^* = 10$ cylinder exhibits little or no response. Although the primary response region, $4.5 < V_r < 6.75$, is wider than for the $m^* = 50$ cylinder, the maximum r.m.s. response amplitude achieved is only marginally greater, $Y_{\text{r.m.s}} = 0.34$ at $V_r = 5.5$. The $m^* = 10$ cylinder's secondary responses, which are centred on $V_r = 7.25$, 8.0, 9.25 and 10.75, cover a wider range of reduced velocities than those of the $m^* = 50$ cylinder. As in the primary response region, the cylinder's maximum r.m.s. response amplitude through the secondary response region is relatively unaffected by the decrease in mass ratio; $Y_{\text{r.m.s}} \approx 0.12$ for $m^* = 10$. The most prominent of the $m^* = 10$ secondary responses, which is centred on $V_r = 10.75 \approx 2/\text{St}$, covers a similar width of reduced velocities, $10.0 < V_r < 11.75$, as are covered by the cylinder's primary response.

At higher reduced velocities, $V_r \geqslant 11.75$, the cylinder exhibits a low-amplitude oscillation, $Y_{\text{r.m.s}} \approx 0.03$. The cylinder maintains this low amplitude of oscillation at all higher reduced velocities simulated in this study. In the present text a response, such as that described above, that is maintained at an approximately constant oscillatory amplitude for all reduced velocities above some threshold is referred to as the cylinder's *tertiary response*.

Reducing the cylinder's mass ratio still further to $m^* = 5$ results in a further widening of both the primary and secondary response regions. The $m^* = 5$ cylinder exhibits a discernible response at all reduced velocities above $V_r \approx 4.0$ and achieves a maximum r.m.s. response of $0.33D$ at $V_r = 5.5$, which is similar to the maximum response achieved by the $m^* = 10$ and 50 cylinders. The primary response region, $4.0 < V_r < 7.25$, has widened to the point that its upper extremity is encroaching upon the lower extremity of the secondary response region. The $m^* = 5$ secondary responses, which are centred on $V_r = 7.5$, 8.25, 9.25, 11.25 and 13.25, attain peak r.m.s. responses of between $0.11D$ and $0.13D$. As was previously observed for the $m^* = 10$ cylinder, the widest of the secondary responses, $10.0 < V_r < 12.75$, is centred on $V_r = 11.25 \approx 2/\text{St}$. In its tertiary response region, $V_r \geqslant 13.75$, the $m^* = 5$ cylinder exhibits an r.m.s. response of $0.05D$, which is greater than that observed for the $m^* = 10$ cylinder.

There are significant changes in the cylinder's vibrational behaviour on decreasing its mass ratio from 5 to 2. The $m^* = 2$ cylinder exhibits no clear secondary responses and the primary and tertiary response regions appear to blend into each other somewhere between $V_r = 9.0$ and 11.0. The primary response region, $3.5 < V_r \lesssim 10.0$, is wider than for all of the higher mass ratio cylinders considered. The cylinder achieves a maximum r.m.s. response of $0.35D$ at $V_r = 5.5$. For reduced velocities above $V_r \approx 11.0$ the tertiary response region appears to be well established and the cylinder achieves an approximately constant amplitude of oscillation of $Y_{\text{r.m.s}} \approx 0.15$.

The lowest mass ratio cylinder considered, $m^* = 1$, exhibits a response that is substantially different from those of the higher mass ratio cylinders considered. The $m^* = 1$ cylinder exhibits a significant response at all reduced velocities above $V_r \approx 2.75$. On increasing V_r past 2.75, the cylinder's response rises sharply until a maximum r.m.s. response of $0.35D$ is achieved at $V_r = 5.75$. Following its maximum the r.m.s. response only falls off slightly and remains above $0.3D$ at all higher reduced velocities simulated. There are no secondary responses for the $m^* = 1$ cylinder, and the boundary between the primary and tertiary response regions cannot be clearly identified.

3.2. Excitation and response frequencies

The excitation and response frequencies, f_v and f_o respectively, experienced by the cylinder are presented in Fig. 2 for three representative mass ratios: 50, 5 and 1. These frequencies were identified as the most energetic frequencies in the spectra of the cylinder's lift coefficient and response. Also shown in the figure are the cylinder's in vacuo natural frequency of vibration, f_n, and the variation of the stationary cylinder's natural (Strouhal) shedding frequency, f_s, which was determined using the present numerical method. Where the cylinder exhibits little or no response, i.e. at low reduced velocities for all mass ratios and high reduced velocities for high mass ratios, vortex shedding is found to occur at or close to the Strouhal frequency, i.e. $f_v \approx f_s$, and any low amplitude oscillations that do occur are found to be most energetic at the excitation frequency, i.e. $f_o = f_v \approx f_s$.

3.2.1. Primary response region

As the flow speed past the $m^* = 50$ cylinder is increased and V_r approaches 1/St, the cylinder's amplitude of oscillation rises sharply and the vortex shedding frequency jumps up and locks-in to the cylinder's frequency of oscillation at or close to the cylinder's natural frequency, i.e. $f_v = f_o \approx f_n$. The fluid maintains this shedding frequency

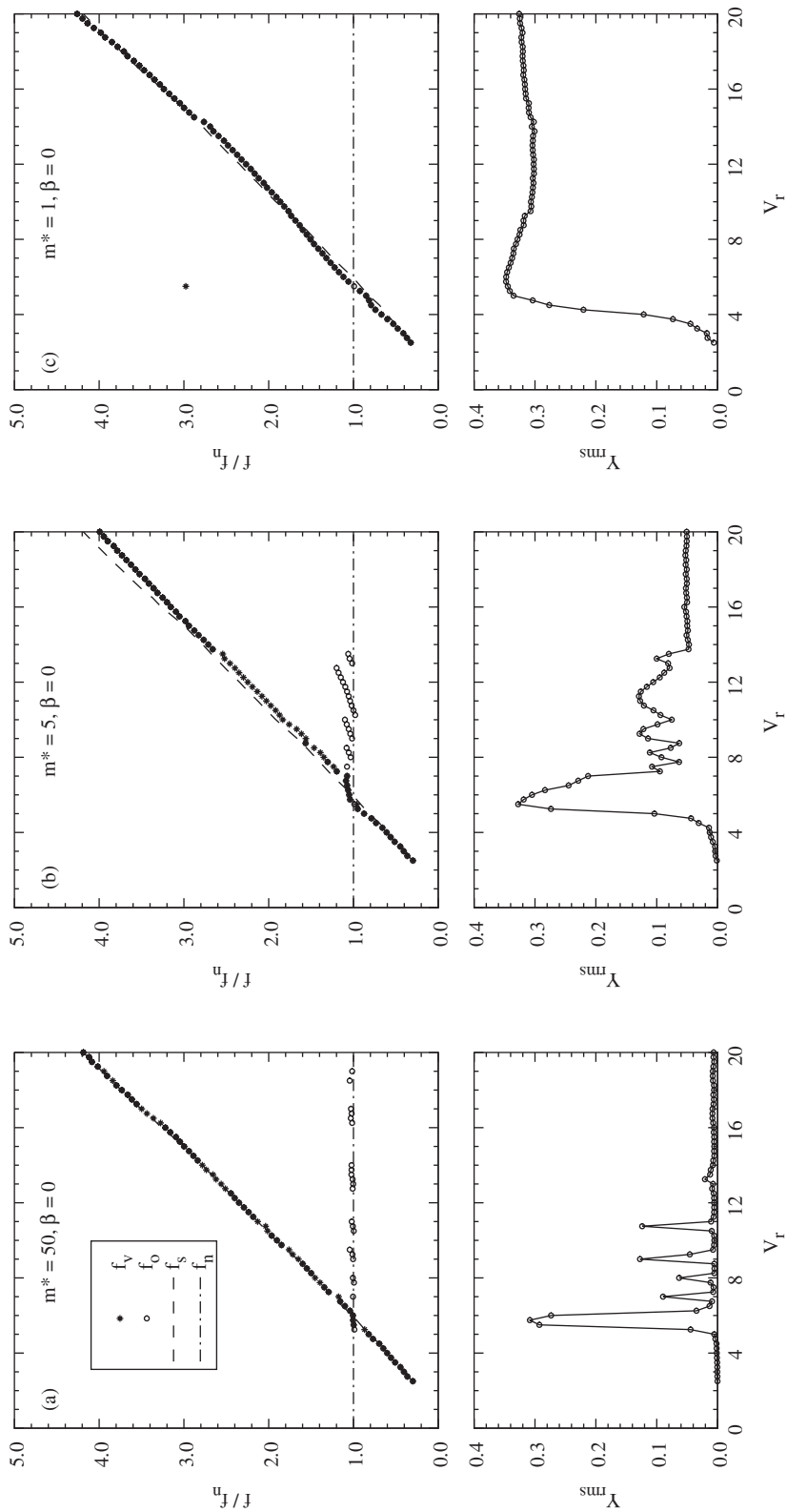

Fig. 2. Root-mean-square response amplitudes, $Y_{\mathrm{r.m.s}}$, excitation and response frequencies, f_v/f_n and f_o/f_n, of transversely vibrating circular cylinders: (a) $m^* = 50$, $\beta = 0$; (b) $m^* = 5$, $\beta = 0$ and (c) $m^* = 1$, $\beta = 0$.

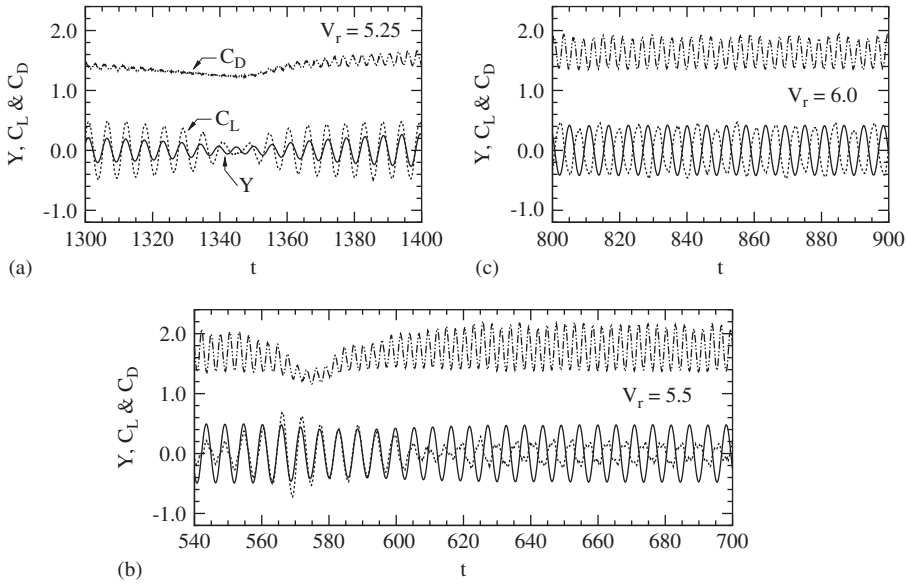

Fig. 3. Time traces of the response, Y, and of the lift and drag coefficients, C_L and C_D, of a transversely vibrating circular cylinder, $m^* = 10$ and $\beta = 0$: (a) $V_r = 5.25$; (b) $V_r = 5.5$ and (c) $V_r = 6.0$.

with increasing V_r until the response amplitude falls away rapidly, at which point the vortex shedding and oscillatory frequencies return to the Strouhal frequency. The departure of the shedding frequency from and its subsequent return to the Strouhal frequency describe the so-called 'lock-in step', which is a characteristic of moderate to high-mass-ratio VIV. Towards the peripheries of the primary response region the cylinder exhibits multiple frequency modulated (or beating) responses.

As the mass ratio is decreased and the width of the primary response region increases so does the width of the primary response lock-in interval, see Fig. 2(b). As well as increasing the width of the lock-in interval, reducing the mass ratio has the effect of altering the frequency at which lock-in occurs. The $m^* = 50$ cylinder responds and sheds vortices at an approximately constant frequency through lock-in, i.e. $\partial f_o/\partial V_r \approx 0$, see Fig. 2(a). However, the frequency at which the lower mass ratio cylinders respond and shed vortices increases with V_r through lock-in, i.e. $\partial f_o/\partial V_r > 0$, see Fig. 2(b). Furthermore, the rate at which f_o increases with V_r through lock-in increases as the mass ratio is decreased. As the ratio of the hydrodynamic forces acting on the cylinder to the cylinder's inertial force (in essence the inverse of the mass ratio) is increased, the fluid is able to exert an increased level of control over the frequency at which the combined fluid and structural system responds. For the lowest mass ratio considered, $m^* = 1$, the fluid is completely dominant over the structure in controlling their joint response frequency and the cylinder responds and sheds vortices at the Strouhal frequency, i.e. $f_o = f_v \approx f_s$, see Fig. 2(c).

Fig. 3 depicts time traces of the response, Y, and the lift and drag coefficients, C_L and C_D, for the $m^* = 10$ cylinder for three selected reduced velocities within the primary response region; $V_r = 5.25$, 5.5 and 6.0. For $V_r = 5.25$, see Fig. 3(a), the cylinder's response and force coefficients exhibit a long-time-period beating behaviour, which is typical of those observed towards the peripheries of each mass ratio cylinder's primary response region. In such cases the response and lift coefficient have significant spectral content at both the cylinder's natural frequency and the Strouhal frequency. This type of beating response occurs where the natural frequencies of the fluid and structural systems are too far apart and the amplitude of vibration too low to force both systems to respond at a single mutually determined frequency. Note that for this reduced velocity and all others prior to resonance, i.e. $V_r < 1/\mathrm{St}$, the cylinder's lift coefficient is relatively in phase with the cylinder's displacement.

The time traces plotted for the cylinder at $V_r = 5.5$, see Fig. 3(b), show a different type of long-time-period behaviour. This case is close to resonance, i.e. $V_r \approx 1/\mathrm{St}$, and the lift force periodically shifts from being in phase with to being π out of phase with the cylinder's displacement. This periodic phase shift is responsible for the long-time-period events seen in the time traces. When C_L is out of phase with the displacement it exhibits a low amplitude, multi-frequency behaviour, which was found to have spectral content at $3f_o \approx 3f_n$ as well as at $f_o \approx f_n$. Spectral content in the lift coefficient at $3f_o$ is observed at reduced velocities close to resonance for all of the mass ratios simulated but is

most prominent for the lowest mass ratios. Indeed at $V_r \approx 1/\mathrm{St}$ the $m^* = 1$ cylinder's C_L spectra is more energetic at $3f_o$ than at f_o, and hence $f_v = 3f_o$ for $V_r = 5.5$, see Fig. 2(c).

For $V_r = 6.0$ the cylinder exhibits a relatively constant amplitude of vibration, see Fig. 3(c). For this case $V_r > 1/\mathrm{St}$ and the lift coefficient, which is also of a relatively constant amplitude, is π out of phase with the displacement. The drag coefficient exhibits a small amount of modulation.

3.2.2. Secondary response region

Four main secondary responses can be identified for each of the cylinders exhibiting secondary responses: $m^* = 5$, 10 and 50, see Fig. 1. The reduced velocities that these responses are centred on, $V_r = 7.25$, 8.0, 9.25 and 11.0, are relatively independent of the cylinder's mass ratio. In general, the higher the reduced velocity at which a secondary response occurs the greater the range of reduced velocities covered by it.

Throughout the secondary response region the fluid sheds vortices at or close to the Strouhal frequency, i.e. $f_v \approx f_s$, and the cylinder oscillates at or near to its in vacuo natural frequency of vibration, i.e. $f_o \approx f_n$, see Figs. 2(a) and (b). However, in this region, neither the displacement nor the lift coefficient are composed of a single frequency and both show spectral content at f_o and f_v. Since $f_v \neq f_o$, the secondary responses cannot be classified as conventional lock-in. The ratio of the vortex shedding frequency to the oscillation frequency, f_v/f_o, is different for each of the secondary responses. For the responses centred on $V_r = 7.25$, 8.0, 9.25 and 11.0, the ratio f_v/f_o takes the values $\frac{7}{6}$, $\frac{8}{6}$, $\frac{10}{6}$ and $\frac{12}{6}$, respectively. The oscillation frequency varies across each secondary response in a manner that enables that response's f_v/f_o ratio to be maintained, and hence $\partial f_o/\partial V_r > 0$ for each secondary response. Furthermore, $\partial f_o/\partial V_r$ shows little dependency on the mass ratio. The widest, in terms of V_r, of the secondary responses is centred on $V_r \approx 11.0 \approx 2/\mathrm{St}$. For this secondary response, vortex shedding occurs at twice the oscillation frequency, i.e. $f_v/f_o = 2$, and hence four vortices are shed per oscillatory cycle.

Time traces of the response, Y, and the lift and drag coefficients, C_L and C_D, are shown in Fig. 4 for the $m^* = 10$ cylinder for four selected reduced velocities: $V_r = 7.25$, 8.0, 9.25 and 11.0. These reduced velocities correspond to the points of maximum response in each of the secondary responses. In all four cases the forces acting on the cylinder, as well as the cylinder's response, show a modulated (or beating) behaviour. As V_r is increased, the frequency ratio f_v/f_o becomes larger and the time period of the cylinder's beating activity becomes shorter. The time traces shown for $V_r = 11.0$ reveal that although the force coefficients are modulated the cylinder's response is not, see Fig. 4(d). For this case the frequency of the excitation force is exactly twice that of the response, i.e. $f_v/f_o = 2$, and the cylinder is able to respond in an un-modulated fashion.

3.2.3. Tertiary response region

At high reduced velocities the cylinder exhibits a tertiary response for $m^* \leqslant 10$, see Fig. 1. Figs. 2(b) and (c) show that in the tertiary response region the cylinder sheds vortices and responds at a common frequency that is at or close to the Strouhal frequency, i.e. $f_o = f_v \approx f_s$. Since $f_o = f_v$ the cylinder's excitation and response in this region can be described as locked-in. Through the locked-in portion of the primary response region the fluid and structural systems respond at a common frequency that lies somewhere between the natural frequencies of the two systems. In contrast, in the tertiary response region the two systems always respond at or near to the fluid natural shedding frequency. The effect of decreasing the mass ratio is to increase the amplitude of the tertiary response rather than to modify the frequency at which it occurs. For the $m^* = 1$ cylinder there is no distinct change in the cylinder's response amplitude or its excitation or response frequencies between the primary and tertiary response regions and consequently the transition between the two cannot be clearly identified.

3.3. Vortex shedding mode

Fig. 5 depicts vorticity contours of the wake aft of the $m^* = 10$ cylinder at four selected reduced velocities: $V_r = 5.5$, 5.75, 9.0 and 11.0. Throughout the range of reduced velocities and mass ratios simulated the cylinder sheds vortices to form a staggered von Kármán-type wake. Where lock-in occurs, i.e. in the primary and tertiary response regions, the vortex shedding mode is of the 2S type, i.e. two oppositely signed vortices are shed per oscillatory cycle. The observed shedding mode is in substantial agreement with those reported from other low-Reynolds-number studies; see, for example, Singh and Mittal (2005).

The cylinder's oscillatory motion increases the transverse separation between the vortices such that the staggered von Kármán wake can become unstable in the middle to far wake region, see Fig. 5. The wake readjusts itself in this region by either rolling-up and coalescing like signed pairs of vortices to form larger vortex structures or by forming pairs of oppositely signed vortices. The secondary response centred on $V_r = 11.0$ is able to develop a regular far wake structure

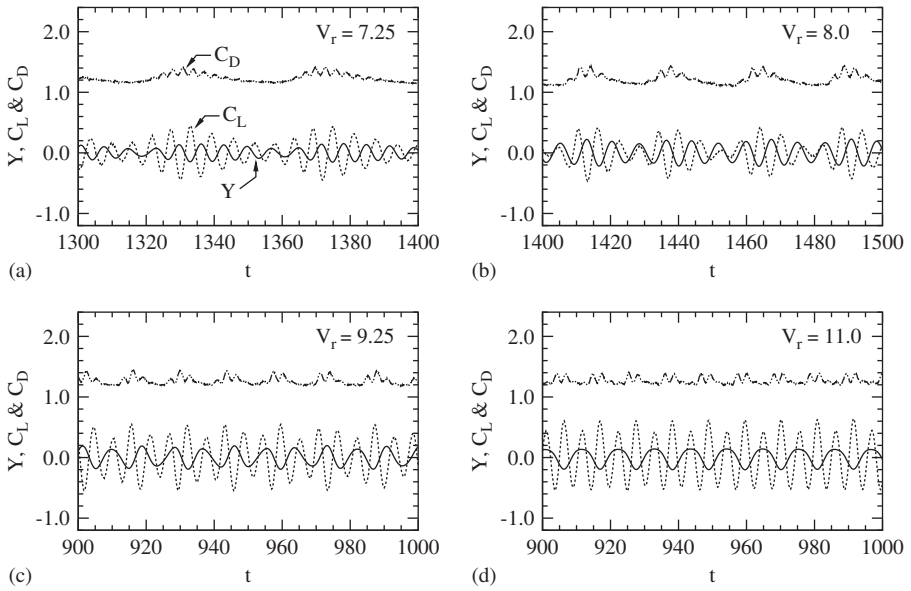

Fig. 4. Time traces of the response, Y, and of the lift and drag coefficients, C_L and C_D, of a transversely vibrating circular cylinder, $m^* = 10$ and $\beta = 0$: (a) $V_r = 7.25$; (b) $V_r = 8.0$; (c) $V_r = 9.25$ and (d) $V_r = 11.0$.

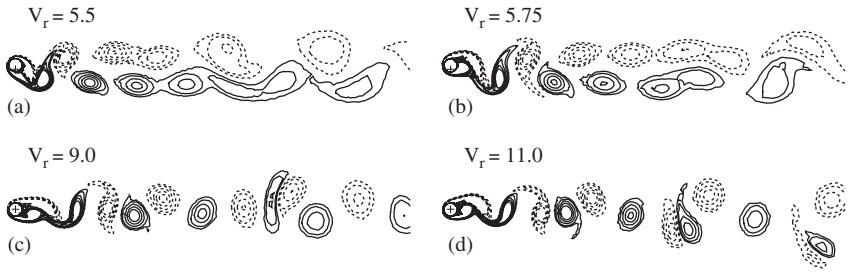

Fig. 5. Vorticity contours in the wake of a transversely vibrating circular cylinder, $m^* = 10$ and $\beta = 0$: (a) $V_r = 5.5$; (b) $V_r = 5.75$; (c) $V_r = 9.0$ and (d) $V_r = 11.0$. Positive and negative contours are depicted using solid and dashed lines, respectively. Contour levels; $\omega = \pm 0.2, \pm 0.4, \pm 0.8, \pm 1.2$ and ± 1.6. Cross-hairs indicate the cylinder's equilibrium position.

that consists of a repeated pattern of two single vortices followed by a vortex pair, see Fig. 5(d). Recall that for this case $f_v/f_o = 2$ and exactly four vortices are shed per oscillatory cycle.

3.4. Phase angles

The variation with reduced velocity of the phase angles, ϕ, ϕ_p and ϕ_f, by which the lift coefficient, C_L, and its pressure and viscous shear stress components, C_{Lp} and C_{Lf}, lead the cylinder displacement are shown in Fig. 6. Phase angles can only be defined where the oscillation and vortex shedding frequencies are equal, and are therefore not reported for all reduced velocities and in particular are not reported for the secondary responses. For phase angles between 0 and π the fluid imparts energy to the oscillating cylinder and acts to excite its motion. For phase angles between $-\pi$ and 0 the fluid extracts energy from the vibrating cylinder and therefore acts to damp its motion. Since in the present investigation $\beta = 0$, there must be no net energy transfer between the fluid and the cylinder once a steady state response has been achieved. Hence, C_L must either be in phase with or exactly π out of phase with Y. On the other hand, ϕ_p and ϕ_f are not constrained in the same manner and can each take on any value between $-\pi$ and π, so long as the energy imparted to the cylinder by the pressure and viscous forces balance each other.

Prior to resonance, i.e. $V_r \lesssim 1/\mathrm{St}$, each cylinder's displacement and lift coefficient are in phase with each other, see Fig. 6. Somewhere in the region of $V_r \approx 1/\mathrm{St}$ each cylinder's lift coefficient abruptly changes to be π out of phase with

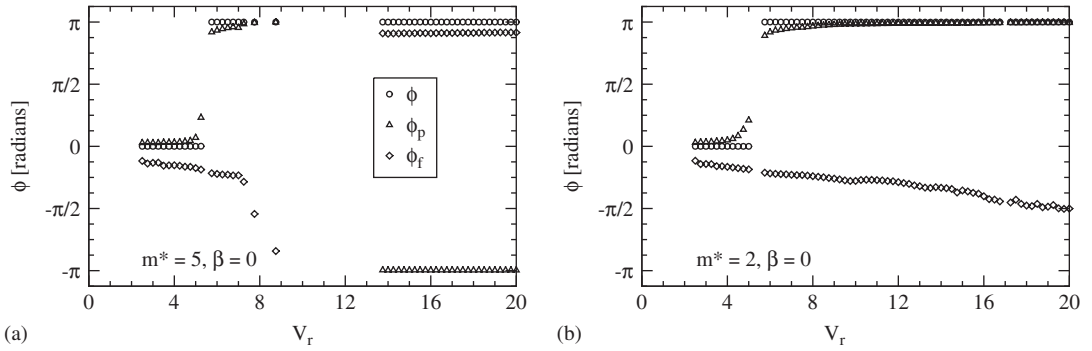

Fig. 6. Phase angles, ϕ, ϕ_p and ϕ_f, by which the lift coefficient and its pressure and viscous shear stress components lead the cylinder's displacement: (a) $m^* = 5$, $\beta = 0$ and (b) $m^* = 2$, $\beta = 0$.

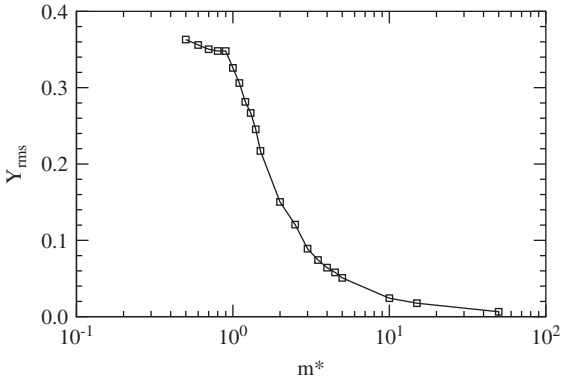

Fig. 7. Root-mean-square response amplitudes, $Y_{\text{r.m.s}}$, as a function of the mass ratio, m^*, for $V_r = 20.0$ and $\beta = 0$.

the cylinder's displacement. For each cylinder, C_L remains out of phase with Y at all higher reduced velocities simulated. The behaviour of the phase angle is observed to be independent of the mass ratio. The change in the phase angle can be associated with a change in the timing of the vortex shedding; from a vortex being shed when the cylinder reaches its maximum displacement on the side opposite to where the vortex was formed, to the vortex being shed when the cylinder reaches its maximum displacement on the side the vortex was formed.

The behaviour of ϕ_p and ϕ_f prior to and through the primary response region is observed to be relatively independent of the cylinder's mass ratio. C_{Lp} exhibits a gradual phase change that occurs slightly in advance of the change in phase of C_L. C_{Lp} starts by leading Y by a small amount and then changes to leading it by almost π through the remainder of the primary response region. C_{Lf} does not change its phase through the primary response region and lags slightly behind the displacement. Hence, through the primary response region the pressure forces act to excite the cylinder's motion and the viscous forces act to provide hydrodynamic damping. An analysis of the pressure and viscous components of the lift coefficient in phase with the cylinder's velocity revealed that in the secondary response region the pressure and viscous forces work in the same manner as in the primary response region, i.e. the excitation due to the pressure forces is balanced by the damping provided by the viscous forces.

The behaviour of ϕ_p and ϕ_f through the tertiary response region is dependent on the cylinder's mass ratio. For the higher mass ratio cylinders, $m^* \geqslant 5$, C_{Lf} leads Y by almost π and C_{Lp} lags behind Y by almost π throughout the tertiary response region, see Fig. 6(a). The lower mass ratio cylinders, $m^* \leqslant 2$, exhibit no further phase changes beyond those that occur around resonance, see Fig. 6(b). Hence, for $m^* \geqslant 5$ excitation and damping are provided by the viscous and pressure forces, respectively, and vice versa for $m^* \leqslant 2$. This observation leads one to question whether the tertiary response region is homogeneous in character for all mass ratios, and whether for the lowest mass ratios considered the tertiary response region is simply an extension of the primary response region.

3.5. Amplitude of response in the tertiary response region

The ability of the fluid to excite the cylinder into significant amplitude responses at high reduced velocities has been further investigated by conducting additional simulations at $V_r = 20.0$ for various m^* and $\beta = 0$. The computed r.m.s. response amplitudes, $Y_{\text{r.m.s}}$, are plotted in Fig. 7 as a function of the cylinder's mass ratio. As has already been observed, the cylinder's r.m.s. response amplitude rises as its mass ratio is decreased. Furthermore, the rate at which $Y_{\text{r.m.s}}$ increases with falling m^* increases as m^* is reduced. Once $m^* < 0.9$ the rate of increase in $Y_{\text{r.m.s}}$ slows and the cylinder only shows a modest further increase in $Y_{\text{r.m.s}}$ between $m^* = 0.9$ and 0.5. The maximum r.m.s. response achieved is $Y_{\text{r.m.s}} = 0.36$ for $m^* = 0.5$, which is similar to the maximum response amplitudes attained in the primary response regions of the five mass ratio cylinders considered earlier.

4. Conclusions

It has been shown by numerical investigation that, at low Reynolds numbers, low-mass-ratio transversely vibrating elastically supported circular cylinders exhibit (at least) three distinct regions of response. The three regions identified in the present text have been classified as the primary, secondary and tertiary response regions.

The primary response region is that normally associated with VIV and occurs in and around resonance. The maximum r.m.s. response amplitude achieved in this region was found to be between $0.31D$ and $0.35D$, and was observed to be relatively independent of the cylinder's mass ratio. Through the central portion of this region the cylinder's oscillation and vortex shedding frequencies were found to be locked-in to each other at a frequency that increased with reduced velocity. Furthermore, the rate of increase of the response and shedding frequencies with reduced velocity was found to increase as the mass ratio was reduced.

Secondary, or super-harmonically excited, responses were found to occur for the higher mass ratios considered, $m^* \geqslant 5$. Multiple secondary responses were exhibited at reduced velocities beyond those covered by the primary response region. The reduced velocities at which the secondary responses occur, and the maximum r.m.s. response amplitude achieved in each, $Y_{\text{r.m.s}} \approx 0.1$, were found to be independent of the cylinder's mass ratio. Across each secondary response, vortex shedding occurs at or near to the Strouhal frequency, whilst cylinder oscillation occurs close to the cylinder's natural frequency of vibration. The oscillation frequency increases across each secondary response, so as to maintain the ratio of shedding to oscillation frequency across that secondary response.

The cylinder's tertiary, or infinite lock-in, response is presently defined as a response that is maintained at an approximately constant amplitude for all reduced velocities above some threshold. Tertiary responses were found to occur for the lower mass ratios considered, $m^* \leqslant 10$. In this region the cylinder responds and sheds vortices at or close to the Strouhal frequency. The effect of reducing the mass ratio is to increase the amplitude of the tertiary response. For the lowest mass ratio considered, $m^* = 1$, there is no discernible change in the cylinder's response or vortex shedding characteristics between the primary and tertiary response regions and one might therefore argue that for very low mass ratios the tertiary response region is simply an extension of the primary response region.

Acknowledgements

R.H.J.W. would like to acknowledge the Royal Academy of Engineering (UK) and the Engineering and Physical Sciences Research Council (UK) who support his position.

References

Anagnostopoulos, P., Bearman, P.W., 1992. Response characteristics of a vortex-excited cylinder at low Reynolds numbers. Journal of Fluids and Structures 6, 39–50.

Feng, C.C., 1968. The measurement of vortex-induced effects in flow past stationary and oscillating circular and D-section cylinders. M.A.Sc. Thesis, University of British Columbia, Canada.

Govardhan, R., Williamson, C.H.K., 2002. Resonance forever: existence of a critical mass and an infinite regime of resonance in vortex-induced vibration. Journal of Fluid Mechanics 473, 147–166.

Sarpkaya, T., 2004. A critical review of the intrinsic nature of vortex-induced vibrations. Journal of Fluids and Structures 19, 389–447.

Shiels, D., Leonard, A., Roshko, A., 2001. Flow-induced vibration of a circular cylinder at limiting structural parameters. Journal of Fluids and Structures 15, 3–21.

Singh, S.P., Mittal, S., 2005. Vortex-induced oscillations at low Reynolds numbers: hysteresis and vortex-shedding modes. Journal of Fluids and Structures 20, 1085–1104.

Toebes, G.H., 1969. The unsteady flow and wake near an oscillating cylinder. ASME Journal of Basic Engineering 91, 493–502.

Willden, R.H.J., 2003. Numerical prediction of the vortex-induced vibrations of marine riser pipes. Ph.D. Thesis, University of London, UK.

Willden, R.H.J., Graham, J.M.R., 2001. Numerical prediction of VIV on long flexible circular cylinders. Journal of Fluids and Structures 15, 659–669.

Williamson, C.H.K., 1996. Vortex dynamics in the cylinder wake. Annual Review of Fluid Mechanics 28, 477–539.

Williamson, C.H.K., Govardhan, R., 2004. Vortex-induced vibrations. Annual Review of Fluid Mechanics 36, 413–455.